IMPEDANCE HAND CONTROLLERS FOR INCREASING EFFICIENCY IN TELEOPERATIONS

C. Carignan, J. Tarrant

ST Systems Corporation
4400 Forbes Blvd.
Lanham, Md. 20706

Abstract

An impedance hand controller with direct force feedback is examined as an alternative to bilateral force reflection in teleoperations involving force contact. Experimentation revealed an operator preference for direct force feedback which provided a better "feel" of contact with the environment. The advantages of variable arm impedance were also made clear in tracking tests where subjects preferred the larger hand controller inertias made possible by the acceleration feedback loop in the master arm. It is expected that the ability to decouple the hand controller impedance from the slave arm dynamics will be even more significant when the inertial properties of various payloads in the slave arm are considered.

NOMENCLATURE

θ_m = master arm position (rad)
I_m = master arm inertia ($kg.m^2$)
I_{md} = desired master arm inertia ($kg.m^2$)
μ_m = master arm viscosity ($kg.m^2.s^{-1}$)
μ_{md} = desired master arm viscosity ($kg.m^2.s^{-1}$)
K_{ma} = master arm acceleration error gain ($kg.m^2$)
K_{md} = master arm artificial damping ($kg.m^2.s^{-1}$)
K_{mp} = master arm position error gain ($kg.m^2.s^{-2}$)
K_{mv} = master arm velocity error gain ($kg.m^2.s^{-1}$)
K_{mf} = force feedback gain to master arm (.)
u_m = master arm control input ($kg.m^2.s^{-2}$)
θ_s = slave arm position (rad)
I_s = slave arm inertia ($kg.m^2$)
μ_s = slave arm viscosity ($kg.m^2.s^{-1}$)
μ_{sd} = desired slave arm viscosity ($kg.m^2.s^{-1}$)
K_{sd} = slave arm artificial damping ($kg.m^2.s^{-1}$)
K_{sp} = slave arm position error gain ($kg.m^2.s^{-2}$)
K_{sv} = slave arm velocity error gain ($kg.m^2.s^{-1}$)
u_s = slave arm control input ($kg.m^2.s^{-2}$)
F_s = contact force on slave arm ($kg.m^2.s^{-2}$)
τ_h = torque from human operator ($kg.m^2.s^{-2}$)
τ_s = torque input to slave arm ($kg.m^2.s^{-2}$)
θ_e = position of slave arm contact (rad)
K_e = environmental stiffness ($kg.m^2.s^{-2}$)
μ_e = environmental viscosity ($kg.m^2.s^{-1}$)
T = sampling period (s)
ZOH = zero order hold (^=sampled data)
COD = computational delay

1. INTRODUCTION

The work presented here explores two control options for hand controllers used in master/slave teleoperation. The first algorithm, bilateral force reflection (BFR), is the more traditional approach and uses position and velocity error signals created when the slave arm contacts an obstacle to generate a force signal in the master arm (see Fig. 1). This system is force reflective since contact will eventually result in a force signal "reflected" back to the master arm. This algorithm also uses a symmetric control structure by which each arm follows the other using the same error signals. Hence the term "bilateral" is also used in describing this form of control.

The other controller used, impedance control with direct force feedback (IDF), does not exhibit the coupling of the master and slave arms as in bilateral control. The only signal fed back from the slave arm to the master arm is a

strain gauge reading proportional to the force on the slave arm. Hence this system is also force reflective but uses direct force feedback rather than position and velocity errors to generate the signal to the master arm. In principle, the contact force has very little to do with the slave arm dynamics unless the object being pushed on is very compliant. Thus the master arm can be considered decoupled from the slave arm. If the position, velocity, and acceleration of the master arm are measured, then the stiffness, viscosity, and inertia of the master arm can be varied using these signals, respectively. Because the designer has full control over the impedance characteristics of the master arm, this form of control has been named "impedance control."

The main advantage of impedance control over bilateral force reflection is that the "feel" of the master arm can be varied at any time. The master arm can be made to feel "heavier" that the slave arm in proximity operations where sudden movement of the slave arm could be disastrous, or feel "lighter" than the slave arm to reduce operator fatigue when transporting massive objects. Similarly, the viscous effect of friction in the gear box could be eliminated, or viscosity could be added if the natural friction does not provide sufficient damping.

Another advantage in IDF control is the presence of direct force feedback to the operator. Instead of receiving pseudoforce information from the robot, the operator can feel exactly what the actual robot arm feels. Not only can force contact be felt, but inertial forces resulting from the slave arm movement can also be sensed because such motion also results in strain on the arm link. Though force feedback is usually considered superior because of the more exact nature of the feedback, it is less stable than its force-reflective counterpart.

Though impedance control is a relative newcomer to the area of teleoperation, its possible advantages in hand controller applications were seen over two decades ago. Gydikov [1] examined the ergonomic impact of varying the inertia of a rotary hand controller mechanically. Subjects were asked to track light stimuli moving at various speeds, and both hand controller velocity and operator pressure on the handle were recorded. His experiments revealed hand tremors of constant frequency when tracking constant velocity targets. Though his purpose was to seek information for formulating operator models, Gydikov's discovery of inertia-dependent hand tremors provided valuable information regarding an important impedance variable in hand controller design.

More recently, Paines [2] developed and tested an impedance hand controller that translated along a linear carriage. His experiments tested the effect of hand controller inertia and viscosity on the ability of an operator to maintain a constant position during a step input or drive the hand controller to some desired position. Though his main purpose was to study the effect of gravity on operator performance (tests were also conducted in neutral buoyancy), he also discovered hand tremors in the velocity data which depended on the inertia and viscosity of the hand controller.

There are many papers on the use of direct force feedback in robot control applications, but relatively few in which a master arm is used to provide the slave arm commands. Hannaford and Anderson [3] conduct master/slave experiments using a configuration similar to ours with fixed impedances. In addition to the force feedback term to the hand controller, however, they retain the position error term in the master arm feedback which we found to detract from the advantages of direct force feedback. The main purpose of their experiments was to verify the accuracy of the human operator model used in their simulations as well as detect parameters pertinent to hand controller design.

Their experiments revealed significant hand controller chattering on impact when only one or two fingers were used to grab the handle, but reduced significantly when the full hand was used. Perhaps even more significantly, it was found that although adding servo level damping to the hand controller had a similar effect to the additional damping provided by the operator's full hand, the system felt "sluggish" to the operator. This facilitated an argument for a control architecture in which the human operator impedance is continuously measured and only the minimum necessary amount of damping be supplied by the hand controller. It is not difficult to argue a position in favor of adjusting the full hand controller impedance using such monitoring.

As mentioned previously, there are many papers which deal with the issue of force control without the added complication of a human operator in the control loop. One such paper by An and Hollerbach [4] provided the inspiration for our force contact experiments with an eccentric cam. Whitney [5] provides a good overview on force, stiffness, and accomodation control for robot applications. The reader is cautioned that these control terms refer to the inputs to the robot arm and not the type of feedback used, e.g. "force control" means the force is commanded not that the force is fed back. Often, all three sensor readings, position, velocity, and force, are fed back to modify the inputs to the robot arm. The reader may also be interested in referring to an excellent paper by Eppinger and Seering [6] on bandwidth limitations in robot force control when reading the analysis section of this report.

2. DYNAMICS

The block diagrams for the BFR and IDF systems when there is no force contact are shown in Figs. 2a and 2b, respectively. Without force contact, the contact sensor will read only the inertial forces from the slave arm rotation, thus the acceleration feedback term in the IDF case. (The gauge actually reads $-(\rho/L)I_s\ddot{\theta}_s$, where ρ is the master arm's radius of gyration and L is the load calibration position; since most of the inertia originates in the handle, $\rho \approx L$.)

The transfer function between the human input torque to the master arm and the commanded input torque to the slave arm is

$$\frac{\tau_s}{\tau_h} = \frac{H_s G_m}{1+H_m G_m+H_s G_s} \qquad \text{[BFR]} \tag{1a}$$

$$\frac{\tau_s}{\tau_h} = \frac{H_s G_m}{1+(1+K_{mf} I_s G_m s^2) H_s G_s} \qquad \text{[IDF]} \tag{1b}$$

For the continuous-time version, the component transfer functions are as follows:

$$H_m = K_{mv}s + K_{mp} \qquad G_m = \frac{1}{I_m s^2 + \mu_m s} \tag{2}$$

$$H_s = K_{sv}s + K_{sp} \qquad G_s = \frac{1}{I_s s^2 + \mu_s s}$$

If there is no arm damping present, (1) reduces to

$$\frac{\tau_s}{\tau_h} = \frac{K_{sv}s + K_{sp}}{I_m s^2 + (\frac{I_m}{I_s}K_{sv}+K_{mv})\,s + (\frac{I_m}{I_s}K_{sp}+K_{mp})} \qquad \text{[BFR]} \tag{3a}$$

$$\frac{\tau_s}{\tau_h} = \frac{K_{sv}s + K_{sp}}{I_m s^2 + (\frac{I_m}{I_s}+K_{mf})K_{sv}\,s + (\frac{I_m}{I_s}+K_{mf})K_{sp}} \qquad \text{[IDF]} \tag{3b}$$

where $I_m=I_s=I$. If the corresponding position and velocity error gains are equal in the BFR case, and K_{mf} is chosen to be unity in the IDF case, then the position and velocity gains for both cases can be determined by

$$K_v = I\zeta\omega_n$$
$$K_p = \frac{1}{2}I\omega_n^2 \tag{4}$$

where ω_n is the desired natural frequency or system "bandwidth" and ζ is the damping ratio.

In the case where the slave arm is in contact with the environment (see Fig. 3), the situation is complicated by the effect of the contact force on the slave arm itself plus the feedback term to the master arm in the IDF case. (Note: we now choose to ignore the inertial force in the sensor dynamics because of the domination of the contact force.) After a considerable amount of block diagram manipulation in which the relay is replaced by unity, one is left with the standard representation shown in Fig. 4 where the plant open-loop transfer function, G, is given by

$$G = \frac{-K_e H_s G_s G_m}{1+(K_e+H_s)G_s} \tag{5}$$

the compensator by

$$H = -K_{mf} + H_m\,(\frac{1}{K_e} + \frac{G_m}{G}) \tag{6}$$

and the component transfer functions by (2). (Note: for the impedance controller, I_m, μ_m, and μ_s are replaced by the

desired quantities, I_{md}, μ_{md}, and μ_{sd} which are attained by using the feedback gains K_{ma}, K_{md}, and K_{sd}, respectively, to alter the natural values.) The steady state response of F_s to an operator step input of magnitude F_H in each of these cases is

$$f_s = -\frac{K_{sp}}{K_{mp}} F_H \qquad \text{[BFR]} \qquad (7a)$$

$$f_s = -\frac{1}{K_{mf}} F_H \qquad \text{[IDF]} \qquad (7b)$$

Thus, if the slave contact force is to match the human input force in steady-state, $K_{mp}=K_{sp}$ in the BFR case and $K_{mf}=1$ in the IDF case.

3. STABILITY ANALYSIS

In formulating the results in this section, the reader should be aware that the system being examined is closed-loop only insofar as the operator input is unaffected by tactile feedback from the master arm and visual feedback from the slave arm. In reality, this is not the case, and we can expect the operator to add a significant amount of damping as well as inertia to the overall system. Our immediate conclusions on stability are therefore only valid for open-loop commands to the master arm when the slave arm is in contact with an object.

It is also important to realize that the actual transfer function for force contact is nonlinear, the simplest being a relay-type model. During experiments, the slave arm will typically bounce upon impact with an object, alternating between free-space motion and force contact. Thus the stability results are only valid for a "velcro" contact situation where the slave arm stays latched to the object. This situation is realistic for cases of fairly compliant surfaces but not for stiffer surfaces. Thus we cannot predict instabilities resulting from impact on a hard surface without resorting to a nonlinear analysis.

A root-locus stability analysis was done for the continuous-time system shown in Fig. 3. The root loci in the BFR case show the closed-loop poles varying as the gain on the master compensation, H_m, is increased from zero to infinity. Figure 5a shows the root loci for a bandwidth of 10 Hz in the BFR case when no natural damping is present ($\mu_m=\mu_s=0$) and the environmental stiffness is $K_e=1000$ N-m/rad where the "bandwidth" refers the system's natural frequency in the freespace case with gains determined by (4).

The conjugate pairs adjacent to the imaginary axis are largely the result of the interaction with the environment and become more oscillatory for larger K_e. These roots will be referred to as the "contact" poles. The roots along the circle close to the origin are the system poles for free-space motion, that is, they are the poles for τ_s/τ_h when no contact force is present, $K_e=0$. This circle increases in size with system bandwidth for constant damping ratios. These poles will be referred to as the "free-space" poles. The BFR case is always stable in the continuous-time case.

The root loci for the IDF case in Figure 5b are very similar to the BFR case except for the finite stability margin on the poles resulting from environmental contact. When K_{mf} is greater than unity in the zero damping case, the system becomes unstable. As expected, the faster response resulting from the use of direct force feedback over position/velocity error has the property of destabilizing the system for higher values of K_{mf}.

Adding damping has the effect of reducing the oscillation in the free-space poles but has little effect on the contact poles. Reducing the environmental stiffness leaves the contact poles still highly underdamped but lower in magnitude while the free-space poles remain relatively unaffected. For high enough reductions in stiffness, the free-space and contact poles may begin to interact. When processing delays are included, the stability is affected dramatically [7]. The system is very unstable for sampling frequencies less than 1000 Hz and environmental stiffnesses on the order of 1000 N-m/rad. Thus without taking into account the effect of the human operator, the system is found to destabilize rapidly when sampling and computational delays are present.

Without changing the model itself, attempts were made to incorporate the effect of the operator by adjusting two existing parameters: the master arm natural damping, μ_m, and the "environmental" damping, μ_e. A test was conducted in which the master arm was moved at a moderate speed until the slave arm impacted a wooden block. Experimental results are shown in Fig. 6 for an environmental stiffness of $K_e = 1000$ N-m/rad. As seen in the

velocity profiles, the master arm displays a minor backlash from the impact whereas the slave arm displays none at all. In the first simulation attempted, the master arm damping was increased to 10 kg-m^2/s and the impact induced instability; the initial bouncing at impact was less than in the undamped case, but then the oscillations began growing unbounded. When instead the environmental damping was increased to 10 kg-m^2/s, the position and velocity profiles shown in Fig. 7 exhibited fair agreement with the experimental results.

The contrasting behavior resulting from increasing the damping in the master arm versus the slave arm can be confirmed by replacing K_e in (5) and (6) by G_e

$$G_e = \mu_e s + K_e \tag{8}$$

and reconstructing the root-loci. Figures 8 and 9 give the results for increasing μ_m and μ_e, respectively, for the case shown in Fig. 5b. Increasing μ_m improves the gain margin by a factor of 20, but the poles still remain highly oscillatory and will destabilize under digital sampling. Increasing μ_e not only stabilizes the system for all values of K_{mf}, it also critically damps the contact poles.

Though the effects of the human operator are undoubtably more subtle than varying a value for the damping (the inertia is also modified, for instance), we can at least infer an interesting result from the previous analysis. It appears that the operator injects damping into the system not at the hand controller but at the slave arm. This is consistent with a fairly well known tenet in flexible body dynamics that collocated damping will always act to stabilize a system, but noncollocated damping may not. Thus it is with our system that damping at the point of contact will stabilize the bouncing caused by force impact.

4. EXPERIMENTAL RESULTS

The single-axis hand controller (SAHC) configuration shown in Figure 10 was used to test the control algorithms presented in the previous section. The apparatus consisted of a set of identical rotary hand controllers driven by a set of PUMA direct drive motors with a peak output torque of 5 N-m. Optical encoders with 3200-line resolution were used to measure the angular position of the motor shafts, and the electronics enhanced this resolution by a factor of four to give 16-bit accuracy in the angle. Strain gauges were mounted on each link and calibrated with weights to give torque data. Piezzo-resistive accelerometers (0-5g) were mounted at the base of the links near the handle to provide acceleration measurements in the IDF tests. Accelerometer and strain gauge signals were sent to a MicroVax via an A/D converter, whereas the encoder readings were sent to a counterboard prior to being read by the MicroVax off a DEC parallel line unit. After the control torques were computed, they were converted to analog drive voltages for the motor op-amps using a 12-bit D/A converter.

The SAHC was used in two different experimental configurations. The first series of tests run investigated the effects of master arm inertia and damping on the tracking ability of the operator. The second series tested the effect of using derived versus direct force feedback on the force perception of the operator. In the tracking experiments, a length of dowel was rotated about a fixed end aligned with the axis of rotation of the slave arm. The operator viewed the slave arm and tracking target through a television monitor (see Figure 11) and rotated the master arm to keep the slave arm following the motion of the dowel. The master arm dynamics were altered to enable four different inertias and two different values of damping to be felt by the operator. The target was also rotated at three different velocities for one set of inertia and damping values to investigate the effects, if any, of target speed on tracking ability.

Autocorrelation analyses of the master arm angular velocity were performed to determine the effects of changing these parameters. It was found that there were oscillations in the velocity, superimposed on a constant value (see Fig. 12). Variations in the amplitude and frequency of these oscillations were observed to depend on the modified inertia and damping of the master arm. The autocorrelation for the case shown in Fig. 12 is given in Fig. 13. In this example, the master arm had an apparent inertia of 0.0086 kg-m^2 and damping of 0.05 kg-m^2/s. Figure 14 gives the average frequency and amplitude of oscillations observed in the autocorrelations for different values of master arm inertia and damping. In all tests, the target speed was 90 deg/s and nonzero damping was 0.05 kg-m^2/s.

The effect of increasing the inertia of the master arm was to decrease both the frequency and amplitude of the oscillations. This is consistent with Gydikov [1] (refer to his Figures 4 and 5), although the actual values are somewhat different because of different hardware configurations. (In his experiments, the operator grasped a handle and rotated a flywheel which involved mainly wrist movement, whereas rotation of the SAHC involved movement

of the entire arm.) The effect of damping was not quite so apparent. For the same inertia, increasing the damping produced an increase in the average frequency of the oscillations although this was not statistically significant. Lower damping and target speeds did however produce significant increases in the average amplitude of oscillation.

The operator seemed to prefer higher master arm inertias when performing the tracking task, as they lessened the "flimsy" feel of the hand controller. Additional damping was not as important because the operator adds damping to the hand controller simply by grasping it. In fact, large values of damping made the motion feel sluggish and required more effort by the operator in controlling the rotations.

In the force experiments, the master arm was rotated until the end of the slave arm came into contact with a rotating circular cam (see Figure 15). The cam had a fixed offset, so that the task for the operator was to maintain a constant contact force on the oscillating surface. Gravity compensation in the control system ensured that the operator had to apply a continuous force to the master arm in order for the slave arm to remain in contact with the cam. The bilateral controller used force feedback derived from the angular position and velocity of the slave arm, and the impedance controller used a direct measurement of the force exerted by the slave arm on the surface. These two controllers were operated at bandwidths of 5 and 10 Hz and the cam rotation at 0.5 and 1 Hz.

In order to obtain a measure of the subject's ability to exert a steady contact force, the standard deviation about a nominal constant value (approximately 0.02 N-m) was calculated. This is illustrated in Figure 16, with the impedance controller (direct feedback) showing the least deviation in all tests and the 10 Hz bandwidth showing better results for both controllers. In all test runs, the average force felt by the operator before responding to the upward motion of the cam was 0.2 ± 0.02 N-m. The difference between the various scenarios was the time taken for this force to be felt, which led to a subsequent delay in the operator response. This delay involved both force perception and reaction time.

At a control bandwidth of 5 Hz, the operator showed little ability to maintain a constant contact force at any cam speed for either controller. For a cam speed of 0.5 Hz and bandwidth of 10 Hz, however, the subject was able to maintain a constant force over about 7/10ths of a cycle when using direct force feedback and 3/10ths of a cycle when using derived force feedback (see Figure 17). The operator's ability greatly diminished at the 1 Hz cam speed when using derived force feedback.

Although the data supports direct force feedback as a more accurate method of contact force perception, the operator could not distinguish between the two controllers during testing. This was because the stiffness of contact felt by the operator is set by the slave arm gains in the IDF case ($K_{mf}=1$) and by the cascaded viscous-spring combination of slave arm and master arm gains in the BFR case. Although the contact force may have felt the same in the two cases, the IDF feedback was exactly the contact force whereas the BFR feedback was corrupted by the secondary "spring" effect of the master arm.

The bandwidth difference, however, was very apparent. At 5 Hz the subject described the surface as feeling "spongy", while at 10 Hz contact was much more sharply defined. The harder contact felt in the 10 Hz case is attributable to the increased proportional/derivative gains used by the slave arm to follow the master arm. Since the PD gains for the slave arm affect the operator feedback in both BFR and IDF control, the operator will perceive a concurrent increase in stiffness of contact when the gains are increased.

5. CONCLUSIONS

The purpose of this research was to test the effect of a variable arm impedance and direct force feedback on the ergonomics and performance of a hand controller to be used in space teleoperation. Both arm inertia and viscosity were to be varied to test their effects on the operator's performance. Direct force feedback was tested against another well known technique from bilateral control which synthesizes a force reflection signal using relative position and velocity errors between the two arms.

Results from the tracking tests reveal a distinct operator preference for a frictionless, high-inertia hand controller. The desire for an undamped hand controller is attributable to the lower effort needed for locomotion. The preference for higher inertias is somewhat less clear, though part of the reason may be better impedance matching between the human arm and the hand controller. Hogan [8] shows that matched impedances provides the most efficient power transmission, a factor which may play the dominant role in an athlete's selection of a tennis racquet or baseball bat.

A less subjective reason may be found by observing the hand tremors present in the tracking tests. The operator found it more difficult to track the target using "lighter" hand controllers because it was more difficult to sense the motion. It is apparent that the subject used tactile information from the inertial forces as well as visual feedback to track the target. This tactile feedback may well be below the operator's force perception threshold to be of much use when using lower inertias.

The observation of inertia-dependent oscillations in the tracking tests yields more than ergonomic information. Their presence reiterates Gydikov's belief that the operator integrates errors and then exerts correcting forces using impulses. Bekey [9] takes this a step further in developing a finite-state model of the human operator. This approach warrants serious consideration, as it may lead to better approaches for modeling the human operator in closed-loop control tasks than the simple damping augmentation approach attempted in the last section.

The effect of direct force feedback was also a critical component of this study, and the force-contact tests yielded some interesting results. Improved performance with increasing bandwidth was not a particularly noteworthy result as it was primarily a function of the gains in the robot arm, not the feedback loop to the master arm. That the force perception was more accurate in the direct force feedback case was significant, however. Tracking a moving surface while attempting to maintain a constant contact force provided a way of quantifying this improvement. Interestingly, the operator was oblivious to his improved performance in the force feedback case. There is, however, a price to pay in stability for this improved performance. Since force feedback is analogous to an acceleration term in the control law, the feedback has a much higher effective gain than its position or velocity counterpart in bilateral control. This effect was easily verified by the root locus analysis, though the differences were somewhat less dramatic in the discrete-time case where the sampling period became a dominating concern [7].

This research showed several advantages of impedance control with direct force feedback over the popular bilateral configuration. These advantages are manifested in both operator perception as well as quantifiable performance measures. A hand controller with either automatic or operator adjustable impedances receiving direct force feedback information will be a strong candidate for space teleoperations involving dextrous manipulators.

ACKNOWLEDGEMENTS

This research was sponsored by NASA Goddard Space Flight Center under contract # NAS-5-28561 (Gary Mosier, project monitor). The authors wish to acknowledge Gary Mosier, Rick Schnurr, George Voellmer, Frank Bauer, and John Croft for their help during various phases of this study. Thanks also go to Reza Akhavan, Larry Alexander, and Tom Feild for their assistance in writing the real-time code for running the hand controllers.

REFERENCES

1. Gydikov, A., "Sampling with Adjustable Frequency in the Hand Movement Control System," Transactions on Human Factors in Electronics, Vol. HFE-8, No. 2, June 1967 pp. 135-140
2. Paines, J. D., "Optimization of Manual Control Dynamics for Space Telemanipulation: Impedance Control of a Force Reflecting Hand Controller," Master of Science Thesis (SSL Rep. #20-87), Massachusetts Institute of Technology, Aug. 1987
3. Hannaford, B., and Anderson, R., "Experimental and Simulation Studies of Hard Contact in Force Reflecting Teleoperation," Proc. IEEE Int. Conf. on Robotics and Automation, San Francisco, April 7-10, 1986
4. An, C. H., and Hollerbach, J. M., "Dynamic Stability Issues in Force Control of Manipulators," Proc. IEEE Int. Conf. on Robotics and Automation, Raleigh, N.C., 1987, pp. 890-896
5. Whitney, D. E., "Historical Perspective and State of the Art in Robot Force Control," Proc. IEEE Int. Conf. on Robotics and Automation, St. Louis, March 25-28, 1985, pp. 262-268
6. Eppinger, S. D., and Seering, W. P., "Understanding Bandwidth Limitations in Robot Force Control," Proc. IEEE Int. Conf. on Robotics and Automation, Raleigh, N.C., 1987
7. Carignan, C., and Tarrant, J., "Impedance Control versus Bilateral Control: A Case Study in Manual Teleoperation," Technical Report, ST Systems Corp., Lanham, Md., Dec. 1988
8. Hogan, N., "Impedance Control of Industrial Robots," Robotics and Computer-Integrated Manufacturing, Vol. 1, No. 12, 1984, pp. 97-113
9. Bekey, G. A., and Angel, E. S., "Adaptive Finite-State Models of Manual Control Systems," IEEE Transactions on Man-Machine Systems, March 1968, pp. 15-20

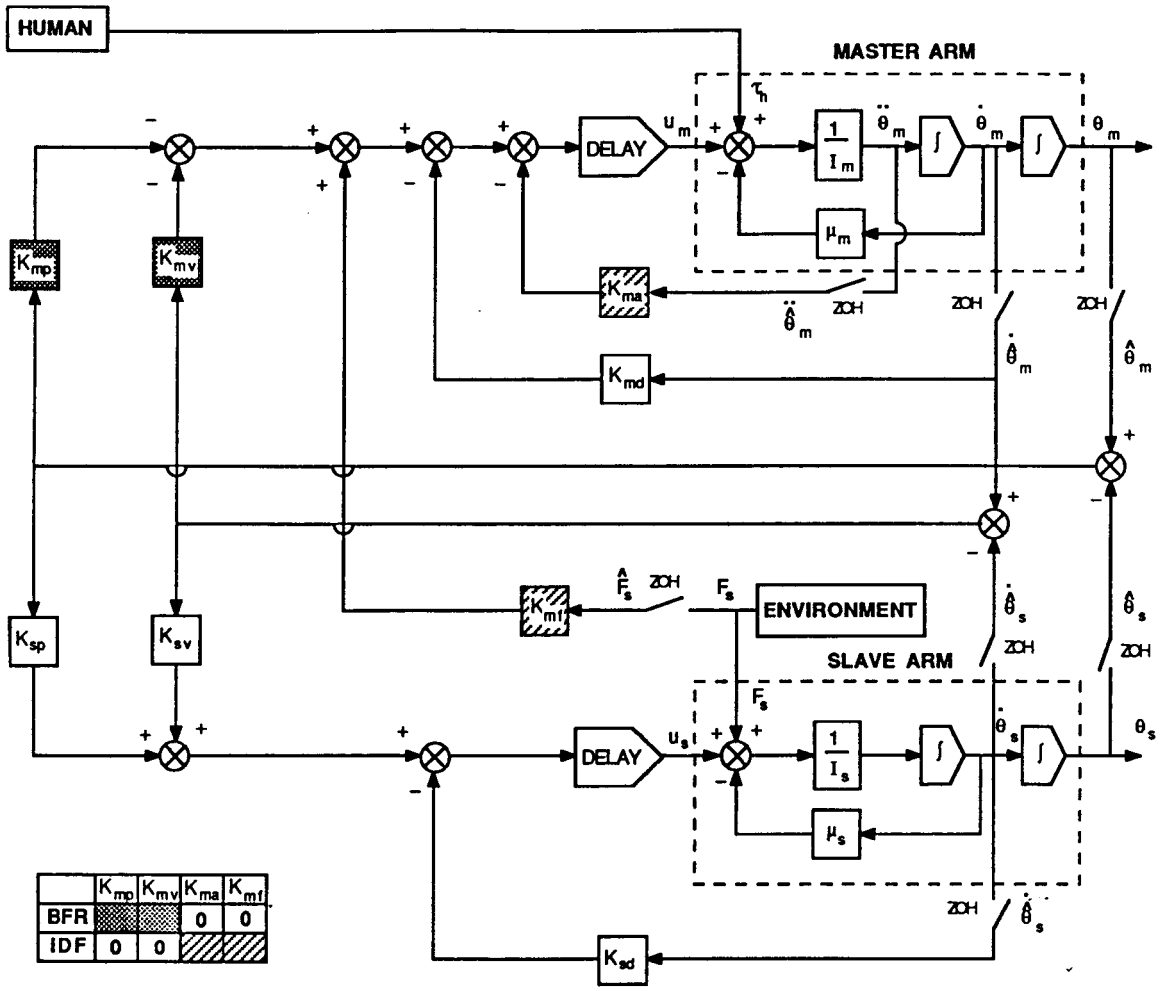

Figure 1: Force reflecting hand controller block diagram.

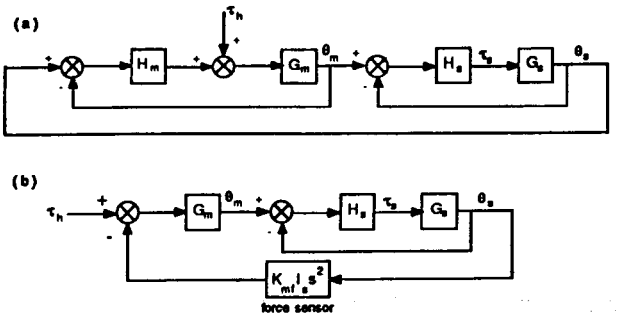

Figure 2: Block diagram for free-space motion in (a) BFR and (b) IDF cases.

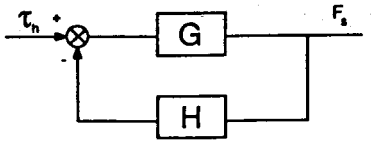

Figure 4: Reduced block diagram for force contact.

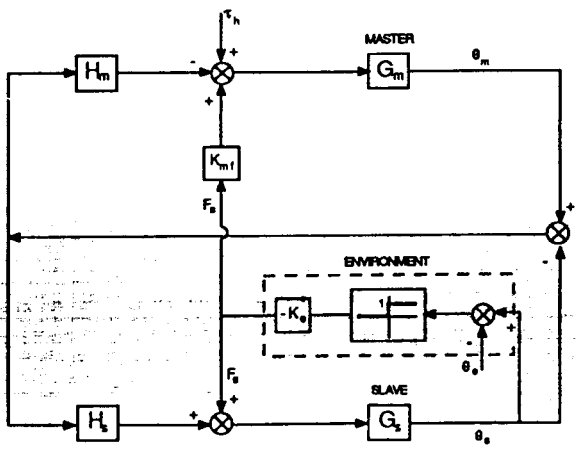

Figure 3: Block diagram for force contact.

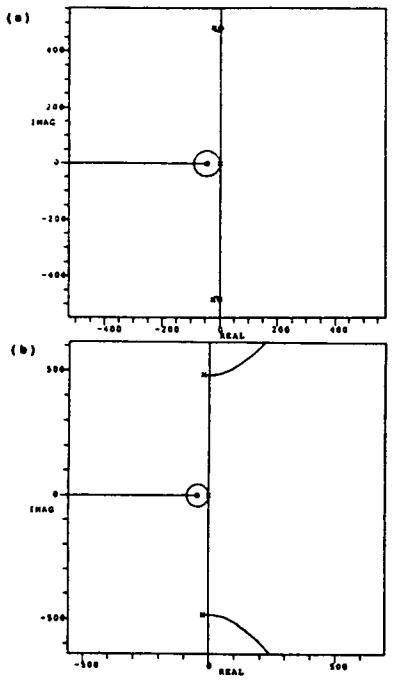

Figure 5: Root loci in (a) BFR case and (b) IDF case for 10 Hz bandwidth and K_e=1000N-m/rad.

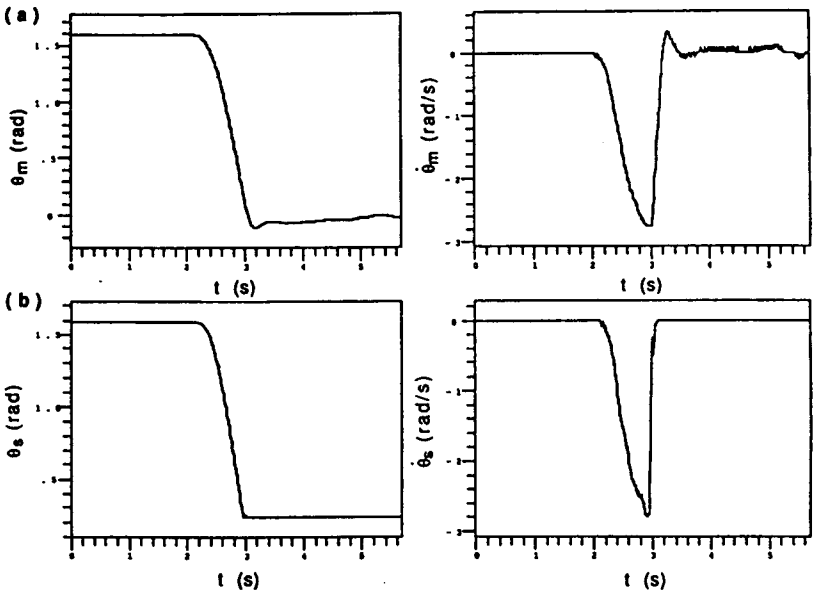

Figure 6: (a) Positions and (b) velocities of master and slave arms during impact experiment.

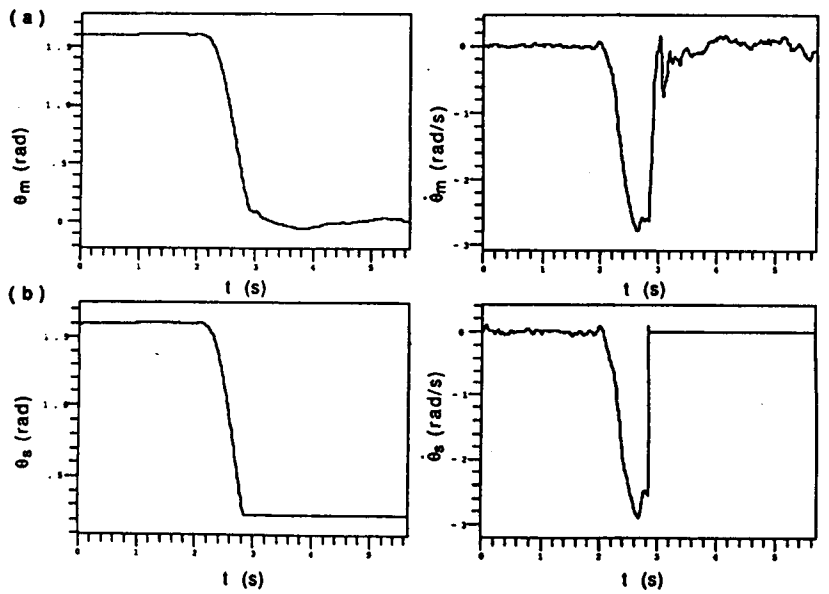

Figure 7: (a) Positions and (b) velocities of master and slave arms during damped environment impact simulation.

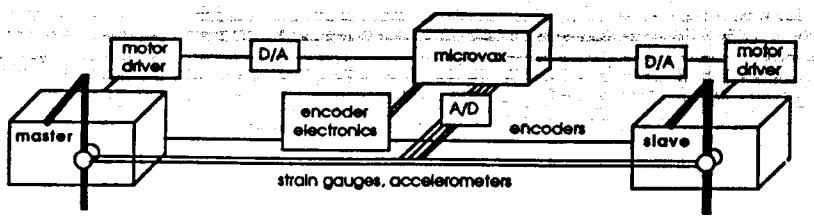

Figure 10: Hardware schematic of single-axis testbed.

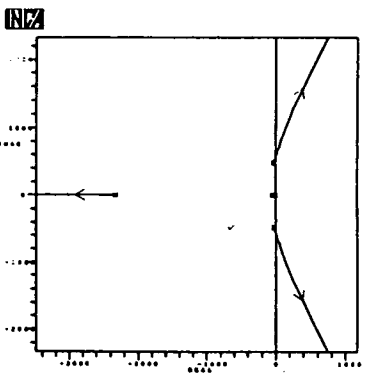

Figure 8: Root locus for master arm damping of 10 kg-m^2/s.

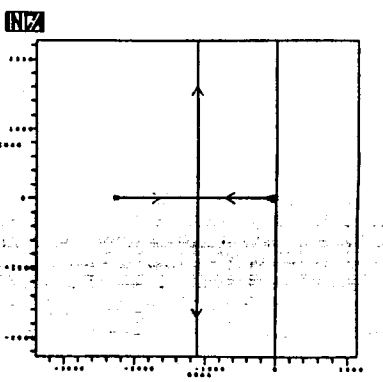

Figure 9: Root locus for damped environment (10 kg-m^2/s).

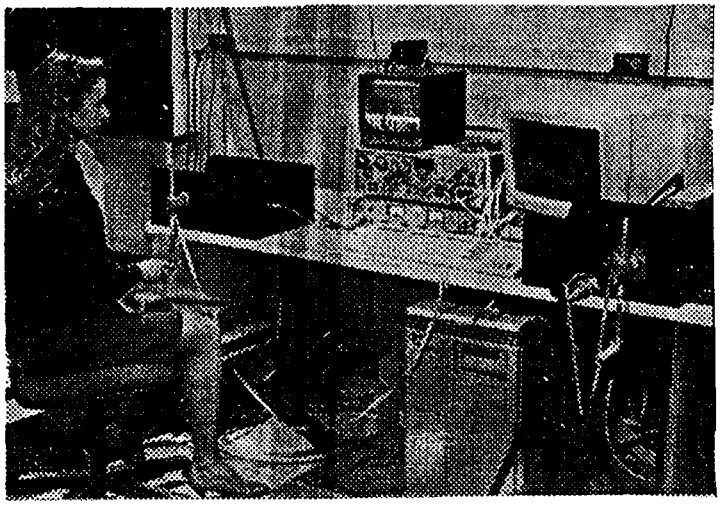

Figure 11: The single-axis hand controller during tracking experiments. The slave arm and tracking target (to right) were viewed by the operator through a television monitor (center).

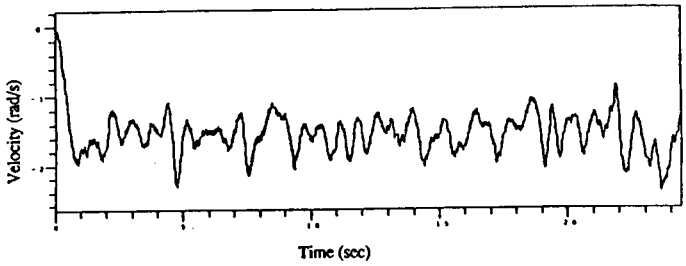

Figure 12: Velocity of master arm during tracking experiment (inertia 0.0086 kg-m^2,damping 0.05 kg-m^2/s).

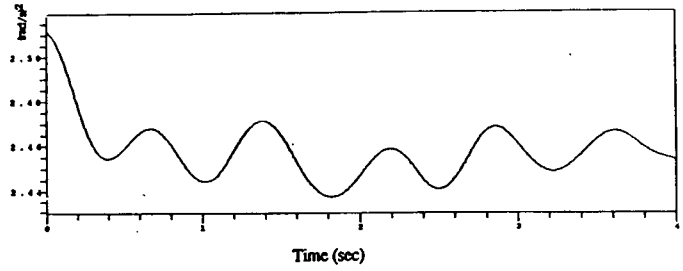

Figure 13: Velocity autocorrelation of master arm during tracking experiment.

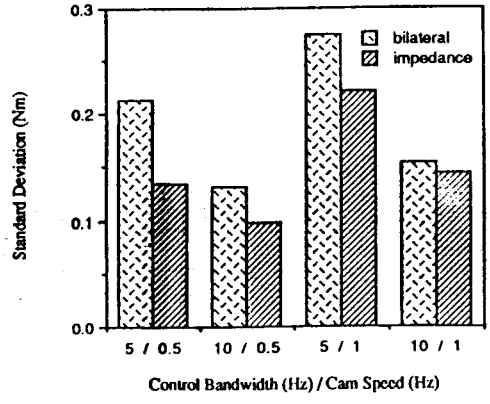

Figure 16: Standard deviation of torque exerted on the cam for various cam speeds and control bandwidths.

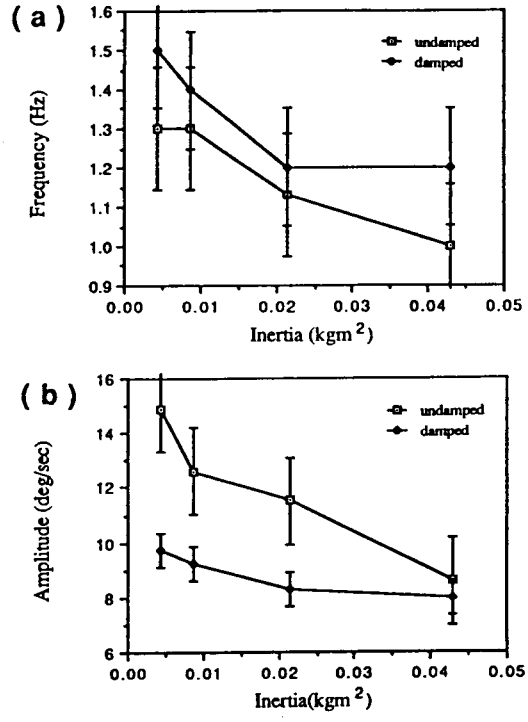

Figure 14: (a) Frequency and (b) amplitude of velocity oscillations observed in tracking experiments.

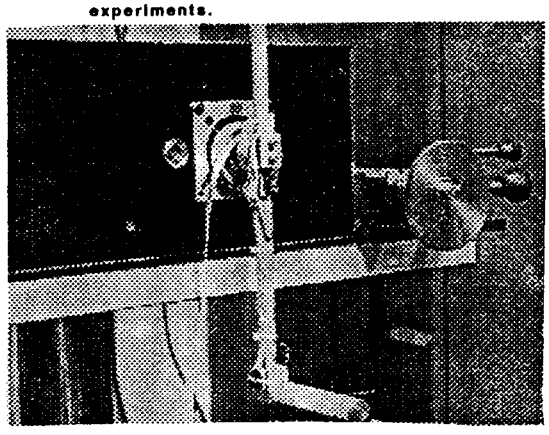

Figure 15: Slave arm and rotating cam (right) used in force experiments.

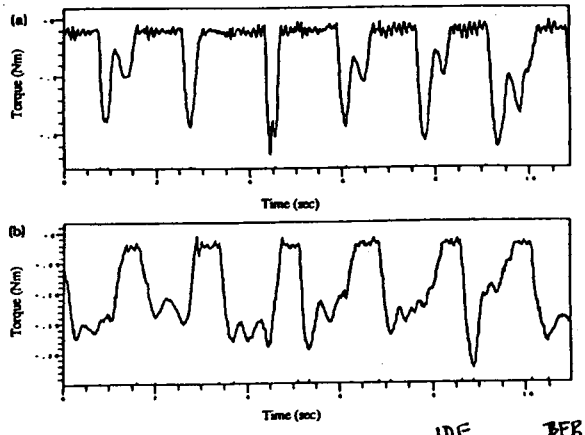

Figure 17: Contact torque on cam for (a) ~~BFR~~ IDF and (b) ~~IDF~~ BFR control for 0.5 Hz cam speed and 10 Hz bandwidth.